

Coexistence of Lithium Metal and Graphite in Anode System for High-Energy Lithium-Ion Batteries

Eunchae Kim, Chaewon Lee, Minju An, Hyosang An, Taeyong Lee,* and Yeonguk Son*

Lithium metal (LM) is a promising anode material for achieving high-energy density owing to its low electrochemical potential and high theoretical capacity. However, LM faces considerable challenges, such as volume expansion and dendrite formation, which induce critical degradation and safety concerns. Recently, the use of both LM and graphite in anode systems is employed as a strategy to mitigate these problems. In this review, electrodes containing both Li and graphite are categorized into

three types based on their dominant Li storage mechanism during cycling, with strategies for each type are discussed. Additionally, the importance of the full-cell parameters necessary to achieve optimal performance with mixed lithium and graphite anodes is discussed. An enhanced understanding of the mechanism of the mixed anode system with lithium and graphite, with a detailed presentation of full-cell parameters, is of significant benefit for the academic and industrial use of lithium-ion batteries.

1. Introduction

The commercialization of Li-ion batteries (LIBs) in the early 1990s marked a revolution in energy storage technology.^[1] Initially developed based on the Li^+ intercalation chemistry using graphite|| LiCoO_2 systems, LIBs have undergone remarkable advancements over the past three decades. Cutting-edge developments in battery technology, including advancements in multifunctional separators, binders, electrolytes, and sophisticated cell packing engineering, have substantially enhanced energy density (ED). The widespread implementation of automated cell-packaging techniques has contributed to a substantial reduction in battery production costs. This progress in LIB technology has facilitated the mass market penetration of smartphones and electric vehicles.^[2–5] In this regard, the market has shown an increasing demand for devices with extended operating times and longer lifespans.^[6–9] However, conventional graphite-based LIBs are approaching their practical ED limits, primarily because of the inherently low theoretical capacity of graphite anodes (372 mAh g^{-1}). Consequently, both industry and academia are exploring new chemistries to overcome the capacity constraints of intercalation-based systems and push the ED boundaries of LIBs.^[10–17]

One promising approach for enhancing the current ED of graphite electrodes is the co-utilization of graphite with high-capacity Si anode materials. Owing to its high specific capacity (3572 mAh g^{-1}) and low operation potential (< 0.4 V vs Li/Li^+), even a small amount of Si in the graphite electrode can significantly boost the ED of cells.^[18–24] In practical applications, Si anodes are physically blended with graphite during the electrode manufacturing process, with current commercial electrodes incorporating up to 8 wt% Si alongside graphite.^[25–30] However, as the Si content increases, the intrinsic volume expansion problem of Si becomes more pronounced. The substantial volume changes of Si anodes (up to 300%) not only induce structural degradation of Si itself but also lead to contact loss between Si and graphite particles, compromising the integrity of the electrode. It also generates new interfaces, promoting the formation of an additional solid electrolyte interphase (SEI) formation.^[31–33] Consequently, these processes lead to irreversible electrode expansion and increased electrode thickness, ultimately reducing the overall ED of the cell. Thus, Si-graphite blending systems currently face constraints in substantially increasing the Si content, which in turn limits their ability to achieve higher EDs.

To overcome these limitations, recent studies have proposed a hybrid Li-graphite (Li–G) system that co-utilizes Li^+ intercalation and Li deposition/stripping chemistry. Li metal (LM) is considered the ultimate anode material as it offers the highest theoretical capacity (3862 mAh g^{-1}) and the lowest reduction potential ($-3.04 \text{ V vs standard hydrogen electrode (SHE)}$) among all known anode materials.^[34–38] Despite these advantages, LM remains impractical for exclusive use as an anode in commercial applications because of dendritic Li plating, which leads to a low Coulombic efficiency (CE) and compromised battery safety.^[39,40] Moreover, Li plating on graphite has been considered undesirable phenomenon.^[41–44] Most of the plated Li grows into needlelike or dendritic structures with a high surface area, making it significantly irreversible. This leads to additional electrolyte decomposition and capacity loss. These dendrites can continue to grow with cycling, eventually causing internal short circuits,

E. Kim, C. Lee, M. An, H. An, Y. Son

Department of Battery and Chemical Engineering

Changwon National University

Changwon Gyeongsangnam-do 51140, Republic of Korea

E-mail: ys8905@changwon.ac.kr

T. Lee

Department of Chemical and Biomolecular Engineering

University of Maryland

College Park

MD, USA

E-mail: mfsmahfr@gmail.com

Y. Son

Department of Chemical Engineering

Changwon National University

Changwon Gyeongsangnam-do 51140, Republic of Korea

which compromise battery safety. Recent studies have explored the hybrid Li–G system not merely to avoid Li plating, but rather to utilize it by inducing reversible Li plating. In this system, graphite not only participates in Li^+ intercalation reactions but also serves as a host for LM deposition in the interparticle space, effectively suppressing dendritic Li plating and improving CE compared to pure LM anodes. In this regard, the hybrid Li–G system is a promising strategy. Graphite engages in Li^+ intercalation reactions and serves as a host for LM deposition in the interparticle space, leading to reduced dendritic Li plating and enhanced CE compared with pure LM anodes. Consequently, the hybrid Li–G system not only enhances the ED of conventional graphite anodes but also mitigates the drawbacks of LM, offering a synergistic and practically meaningful approach for next-generation battery systems.^[34,45–50]

Recently, a deeper understanding of carbon materials (CMs) in the Li-storage dynamics of Li-ion/LM hybrid systems as well as advancements in electrolyte strategies, such as high-concentration electrolytes (HCE) and localized HCEs (LHCE), have significantly enhanced the practicality of hybrid Li–G systems.^[51] Furthermore, progress in roll-to-roll and chemical pre-lithiation techniques has successfully demonstrated the large-scale production of pre-lithiated graphite electrodes, thereby enabling the development of systems with cathodes lacking initial Li sources, such as those using S and O chemistry. Consequently, hybrid Li–G systems are considered highly versatile anode systems that can be applied to various battery configurations, depending on their initial design.

To this end, this review comprehensively discusses the recent progress, characteristics, and challenges associated with different types of hybrid Li–G systems. Understanding and classifying these systems are crucial for understanding the diverse range of cell systems based on hybrid Li–G systems. Furthermore, in full-cell manufacturing, providing accurate information is essential because numerical changes are sensitive to the parameters

and ED calculation methods. However, many studies do not adequately mention the full-cell fabrication conditions or provide information regarding performance, especially ED. To emphasize their significance, we provide the performance metrics for the full-cell used in the hybrid systems.

2. Comparison of Promising Anodes

The LM anode undergoes degradation owing to volumetric expansion and SEI layer formation, similar to the Si anode; it also poses a significant risk of Li dendrite growth. Nevertheless, LM anodes have the potential for a significantly higher capacity than Si anodes. The known theoretical capacities of Si and LMs are 3572 and 3862 mAh g⁻¹, respectively, calculated based on the following electrochemical reactions^[52–54]



The reaction at the Si anode is reduction (during charging in the full-cell), and that at the LM anode is oxidation (during discharging in the full-cell).^[55–58] Considering the reduction of the LM anode, which is an anode-free concept, its theoretical capacity is infinite.^[59–63] The aforementioned theoretical capacities of the Si anode based on reduction and LM anode based on oxidation do not have a large difference.^[64–68] However, when comparing the theoretical capacities under the same charging (reduction) conditions, the theoretical capacity of the LM anode is much higher than that of the Si anode.^[69–72]

To prevent degradation reactions (including volume expansion and continuous SEI formation) in Si anodes,^[73–77] complex synthesis processes are required in addition to the material design of diverse morphologies and composites. In contrast, recent studies



Eunchae Kim is a researcher in the Department of Chemical Engineering at Changwon National University. She received her B.S. and M.S. degrees in Chemical Engineering from Changwon National University, specializing in secondary battery chemistry. Her research focuses on the development of high-energy lithium-ion batteries, including (i) the optimization of silicon-graphite anodes, (ii) the development of anode-free materials, and (iii) electrochemical analysis.



Taeyong Lee is a postdoctoral associate in Department of Chemical and Biomolecular Engineering at University of Maryland, College Park. He received his B.S. and Ph.D. degrees from School of Energy and Chemical Engineering at Ulsan National Institute of Science and Technology in 2021. He conducted postdoctoral research at Seoul National University in the field of lithium-ion batteries from 2021 to 2023. His research interests include (i) the development of anode materials, (ii) electrode design, and (iii) electrolyte engineering for high-energy lithium-ion batteries.



Yeonguk Son is an assistant professor in the Department of Chemical Engineering at Changwon National University. He earned both his B.S. and Ph.D. in energy and chemical engineering from UNIST. From 2018 to 2021, he worked as a research associate in the Department of Engineering at the University of Cambridge. His research focuses on (i) developing electrode materials for high-energy storage, (ii) employing advanced analysis techniques for electrode materials, and (iii) designing electrodes and cells for high-energy lithium-ion batteries.

have suggested that for LM anodes, degradation reactions can be controlled by the application of an ultrathin coating layer or through electrolyte design.^[78–81] This indicates that hybrid Li–G systems may offer a more cost-effective and practical alternative to Si–graphite anodes as a next-generation anode material. Notably, hybrid Li–G systems provide more versatile design strategies, such as the use of pre-lithiated graphite, electrolyte modifications to promote stable Li layer formation, and the use of graphite layers to protect LM.

3. Mixed Li–G Systems

Recently, several systems have been reported to effectively utilize graphite and Li and create new anode systems that improve the ED by maximizing the advantages of both materials while complementing their respective weaknesses. One effective method involves plating Li onto the pores of a graphite anode. Schematic illustrations of the extent of Li plating within the graphite pores at 0%, 50%, and 100% are shown in Figure 1. Based on this, we calculated the changes in capacity, gravimetric ED (GED), and volumetric ED (VED).

The graphite anode composition was set with an active material (AM), a binder material (BM), and a CM in a 90:5:5 weight ratio and an electrode density of 1.6 g cm^{-3} . The areal capacity of the anode was calculated to achieve a negative/positive (N/P) ratio of 1.05 (Equation (3)). Note that Q_{re} is the reversible capacity and Q_{irr} is the irreversible capacity. We assumed that $\text{LiNi}_{0.8}\text{Co}_{0.1}\text{Mn}_{0.1}\text{O}_2$ (NCM811) was used as the cathode, with an AM ratio of 90%, electrode density of 3.0 g cm^{-3} , areal capacity of 3.3 mAh cm^{-2} ,

and a cutoff voltage of 4.3 V. The initial CEs (ICEs) of the anode and cathode were set to 85% and 90%, respectively.

$$\text{N/P ratio} = \frac{\text{Anode } (Q_{\text{re}})}{\text{Cathode } (Q_{\text{re}} + Q_{\text{irr}}) - \text{Anode } (Q_{\text{irr}})} \quad (3)$$

The gravimetric capacity of graphite was 360 mAh g^{-1} , and the volumetric capacity of Li was 2061 mAh cm^{-3} . Using these values, along with the electrode density and true densities of AM, BM, and CM, the calculated porosity of the graphite electrode was 24.8% (Equation (4)).^[34,82]

$$\text{Electrode porosity (\%)} = 1 - \frac{\text{electrode density}}{\frac{1}{\sum \left(\frac{\text{material ratio}}{\text{true density}} \right)}} \quad (4)$$

We calculated the gravimetric capacity of the hybrid Li–G electrode according to the degree of Li plating in the pores, ranging from 0% to 100% (Equation (5)).^[34] The true densities of graphite, CMC, SBR, and Super-P are 2.25, 1.95, 1.5, and 0.9 g cm^{-3} , respectively.

$$\begin{aligned} \text{Li–G capacity } (\text{mAh g}^{-1}) \\ = & \frac{\text{Volumetric capacity (lithium)} \times \text{porosity} \times \frac{x}{100}}{\text{AM ratio} \times \text{electrode density}} \\ & + \text{Gravimetric capacity (graphite)} (0 \leq x \leq 100) \end{aligned} \quad (5)$$

Electrode loading, thickness, and voltage were calculated based on the capacity determined by the extent of Li plating. The voltage of the hybrid Li–G system half-cell was derived using Equation (6), with the average voltages of graphite and Li set to 0.13 and 0 V, respectively.^[83]

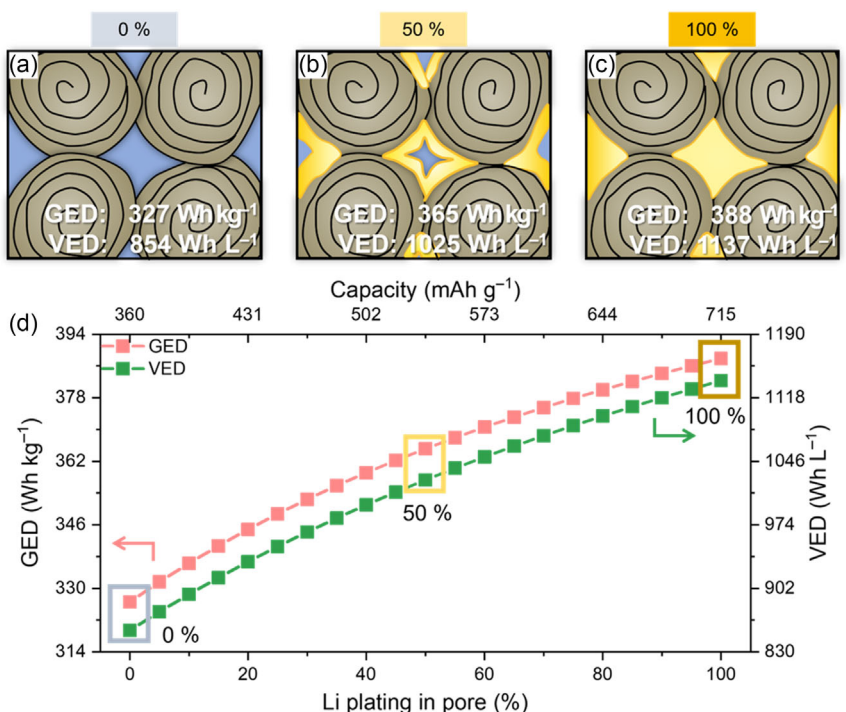


Figure 1. Schematic illustration of Li plating in graphite anode pores at a) 0%, b) 50%, and c) 100%. d) Anode capacity, specific energy (pink), and energy density (green) of the Li plating in the graphite anode.

$$\text{Anode voltage (V)} = \frac{\text{specific capacity (G)}}{\text{Li - G capacity}} \times \text{voltage (G)} + \frac{\text{specific capacity (Li)}}{\text{Li - G capacity}} \times \text{voltage (Li)} \quad (6)$$

Finally, GED and VED were calculated at the electrode level using a full-cell configuration. We assumed that Cu and Al foils with areal weights of 7.07 and 2.65 mg cm⁻² and thicknesses of 8 and 10 µm, respectively, were used as the current collectors.^[34,82]

In a full-cell, the voltage is calculated as a variable dependent on the anode voltage (Equation (7)).^[83] The ICE of the full-cell was predicted based on the calculated Q_{re} and Q_{irr} of the cathode and anode (Equation (8)).

$$\text{Full cell voltage (V)} = \text{cathode voltage} - \text{anode voltage} \quad (7)$$

$$\text{ICE of Full cell (\%)} = \frac{\text{Cathode } (Q_{\text{re}} + Q_{\text{irr}}) - \text{Anode } (Q_{\text{irr}})}{\text{Cathode } (Q_{\text{re}} + Q_{\text{irr}})} \times 100 \quad (8)$$

The GED and VED values, which correspond to the degree of Li plating within the graphite electrode pores, were determined using Equation (9) and (10).^[82,84]

$$\begin{aligned} \text{GED (Wh kg}^{-1}\text{)} &= \text{specific capacity (NCM811)} \\ &\times \text{full cell voltage} \times \text{AM ratio} \\ &\times \frac{\text{mass loading (cathode)}}{\text{mass loading (cathode + anode)} + \text{areal weight (Cu + Al foil)}} \\ &\times \frac{\text{ICE of full cell}}{\text{ICE of cathode half cell}} \end{aligned} \quad (9)$$

$$\begin{aligned} \text{VED (Wh L}^{-1}\text{)} &= \text{specific capacity (NCM811)} \\ &\times \text{full cell voltage} \times \text{AM ratio} \\ &\times \frac{\text{mass loading (cathode)}}{\text{mass thickness (cathode + anode + Cu foil + Al foil)}} \\ &\times \frac{\text{ICE of full cell}}{\text{ICE of cathode half cell}} \end{aligned} \quad (10)$$

As the proportion of Li plating within the pores of the graphite electrode increased, both GED and VED increased. At 0% Li plating (i.e., using a graphite-only anode), the GED and VED values were 327 Wh kg⁻¹ and 854 Wh L⁻¹, respectively (Figure 1d). When the Li plating was 50% and 100%, the GED was 365 and 388 Wh kg⁻¹, and the VED was 1025 and 1137 Wh L⁻¹, respectively. These calculations demonstrate that additional Li plating on the graphite electrode enables a higher ED.

Similar to the enhanced ED achieved by Li plating on graphite anodes, Li can be used with graphite to improve battery performance using various related strategies. We introduce these strategies by systematically categorizing them. The hybrid Li-G system can be divided into three main categories: 1) using LM for the pre-lithiation of a graphite anode (LM@Prelithi-G), 2) using LM as the capacity-enhancing agent of the graphite anode (LM@Capacity-G), and 3) using a protective graphite buffer matrix for LM anodes (G@Matrix-LM). LM@Prelithi-G (Figure 2a) refers to

the use of Li through a pre-lithiation strategy in graphite-based anodes, where intercalation/deintercalation dominates as the primary Li storage mechanism, leading to an improved ICE. LM@Capacity-G (Figure 2b) can utilize not only the capacity of graphite but also the capacity of the added LM through the intercalation/deintercalation reaction of graphite and the plating/stripping reaction of LM. Finally, G@Matrix-LM (Figure 2c) involves utilizing graphite as a protective matrix in LM anodes, where Li plating and stripping dominate as the main Li storage mechanism, helping to prevent the irreversible behavior of LM. Therefore, while it is generally true that LM@Prelithi-G primarily utilizes the capacity of graphite and G@Matrix-LM mainly relies on the capacity of Li, classifying these categories based on their strategies rather than strictly quantifying the amount of Li used provides a clearer distinction. The subsequent sections provide examples to explain these three systems in detail.

3.1. LM@Prelithi-G

The ICE of anodes is typically low due to several factors, including the formation of an SEI caused by electrolyte decomposition, AM loss resulting from volume expansion, and Li-ion trapping at defective sites. These irreversible Li losses ultimately reduce the ED of LIBs. To overcome this issue, various pre-lithiation strategies have been extensively explored as an effective solution. Different pre-lithiation techniques have been developed to compensate for irreversible Li loss during the initial charge–discharge cycles. These include chemical pre-lithiation, electrochemical pre-lithiation, and the incorporation of active additives. Additionally, constructing a robust and fast ion-conducting SEI can help mitigate Li loss. Among these approaches, pre-lithiation using electrode additives has shown the greatest promise for industrial application due to its simplicity and effectiveness. Over the past decade, pre-lithiation has been widely recognized as a key strategy for minimizing Li loss and enhancing the ED of next-generation LIBs. The additional Li not only serves as a reservoir to compensate for Li depletion caused by anode aging but also reduces the average potential of the negative electrode, thereby increasing the overall cell voltage. As a result, pre-lithiated anodes have emerged as a highly effective solution for improving both the performance and longevity of LIBs.^[85–90]

The fabrication of Li-enriched silicon/graphite (LESG) begins with the preparation of nickel-laden graphite. Pristine graphite is first mixed with a nickel acetate solution, followed by desiccation and thermal reduction to form nickel-laden graphite. This material is then immersed in a LiOH solution, stirred, and subjected to alkaline activation, resulting in the formation of a graphite–nickel–LiOH composite. Subsequent treatment of this composite with H₂SO₄ and deionized water produces Li-rich graphite (LEG), characterized by its porous basal planes. Finally, LEG, nano-silicon particles, and pitch are mixed in tetrahydrofuran solution, and the resulting mixture undergoes spray drying and high-temperature calcination to form LESG (Figure 3a).^[91] The ICE of LESG and silicon–graphite/Li half-cells is 116% and 86.9%, respectively, at a current rate of 0.1 mA g⁻¹. The LESG cell exhibits stable cycling for over 400 cycles, with a

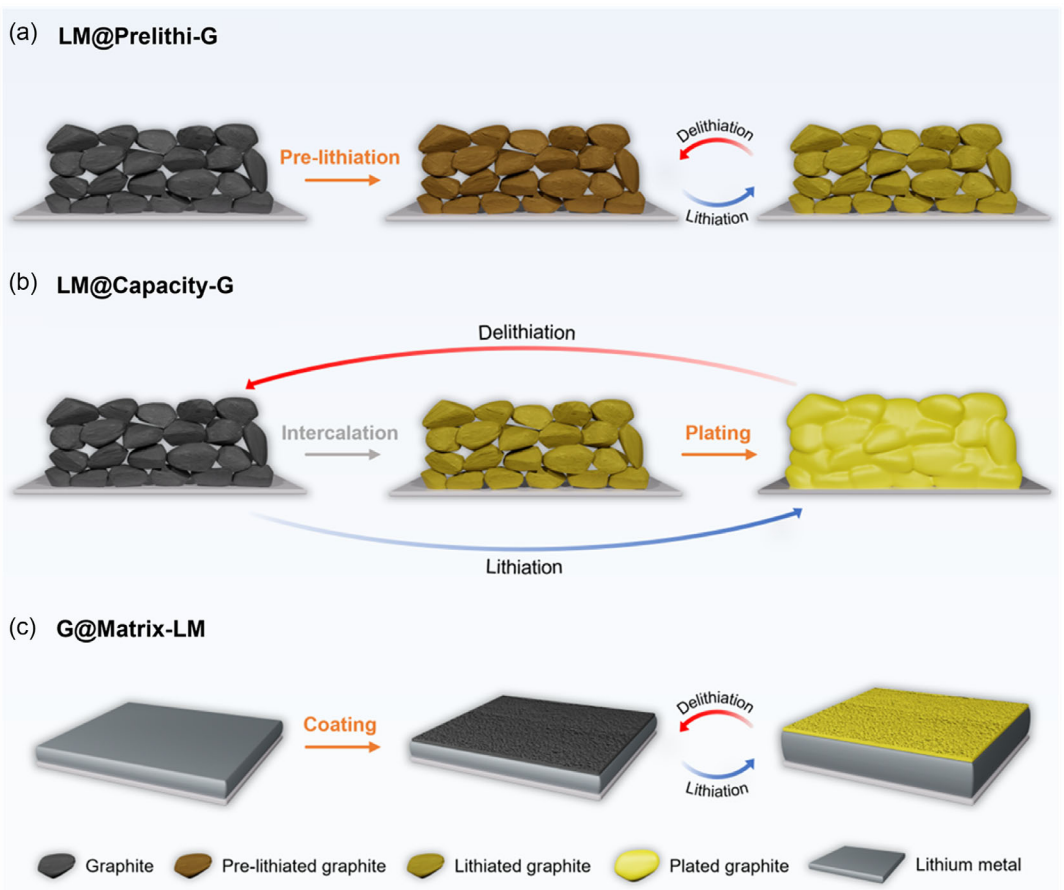


Figure 2. Schematic illustration of the Li-G storage systems: a) LM@Prelithi-G, b) LM@Capacity-G, and c) G@Matrix-LM.

slower capacity decay rate compared to that of a commercial silicon-graphite-based cell. In contrast, the silicon-graphite cell cycles for fewer than 200 cycles, possibly due to the volume expansion of nano-silicon particles, which damages the electrode structure and causes the AM to detach from the current collector.

While the LESG approach integrates Li directly into the anode material through a chemical synthesis route, alternative pre-lithiation strategies have been explored to enhance the initial efficiency and cycle stability of graphite-based anodes. Wang et al. achieved direct contact between 5 wt% stabilized LM powder (SLMP) and a graphite anode, and the subsequent calendering process completed the pre-lithiation.^[92] When comparing a cell containing SLMP (referred to as a “pre-lithiated cell”) to a cell without SLMP (“non-pre-lithiated cell”), the open-circuit voltage (OCV) of the non-pre-lithiated cell was observed to be above 1 V, whereas the pre-lithiated cell exhibited a lower OCV (\approx 0.1 V). Electrolyte decomposition and SEI formation occurred within the voltage plateau (0.6–0.7 V) of the non-pre-lithiated cell. The pre-lithiated cells demonstrated superior efficiency, while maintaining a cycle performance similar to that of the non-pre-lithiated cells (Figure 3b), thereby effectively facilitating spontaneous SEI formation during rest in an open circuit. The pre-lithiated and non-pre-lithiated cells exhibited delithiation capacities of 340 and 320 mAh g⁻¹, respectively. Therefore, the pre-lithiated graphite anode reduced the irreversible capacity

loss and increased the overall capacity by 5%–10%. Compared to non-pre-lithiated cells, the pre-lithiated cells exhibited higher delithiation capacities and improved efficiency, demonstrating the effectiveness of SLMP-assisted pre-lithiation in optimizing anode performance.

Building upon the concept of pre-lithiation via direct Li incorporation, Yang et al. demonstrated the pre-lithiation of graphite using the roll-to-roll method (Figure 3c).^[93] Graphite was applied to a smooth stainless steel surface through slurry coating, and a thin Li layer was electrodeposited onto the Cu foil. Subsequently, calendering was used to transfer the graphite layer from the stainless steel to the Cu foil, resulting in the production of a pre-lithiated electrode. In the pre-lithiated electrode, the Cu foil acts as a current collector, the graphite layer serves as the AM, and the Li layer is designed as a Li source for the pre-lithiation reaction. In the half cell test, a graphite anode pre-lithiated at 30% of the graphite capacity (30preG electrode) showed a higher ICE (99.99%) and lower OCV (0.3702 V) than the bare graphite anode (G electrode). The 30preG and G electrodes had initial delithiation capacities of 317.7 and 304.4 mAh g⁻¹, respectively. The 30preG electrode exhibited better rate capability than the G electrode at 0.1C (348.3 mAh g⁻¹), 0.2C (338.3 mAh g⁻¹), 0.5C (320.7 mAh g⁻¹), and 1C (266.7 mAh g⁻¹). Therefore, the 30preG electrode had a more stable SEI and better ICE and rate performances than the G electrode. The 30preG electrode, pre-lithiated at

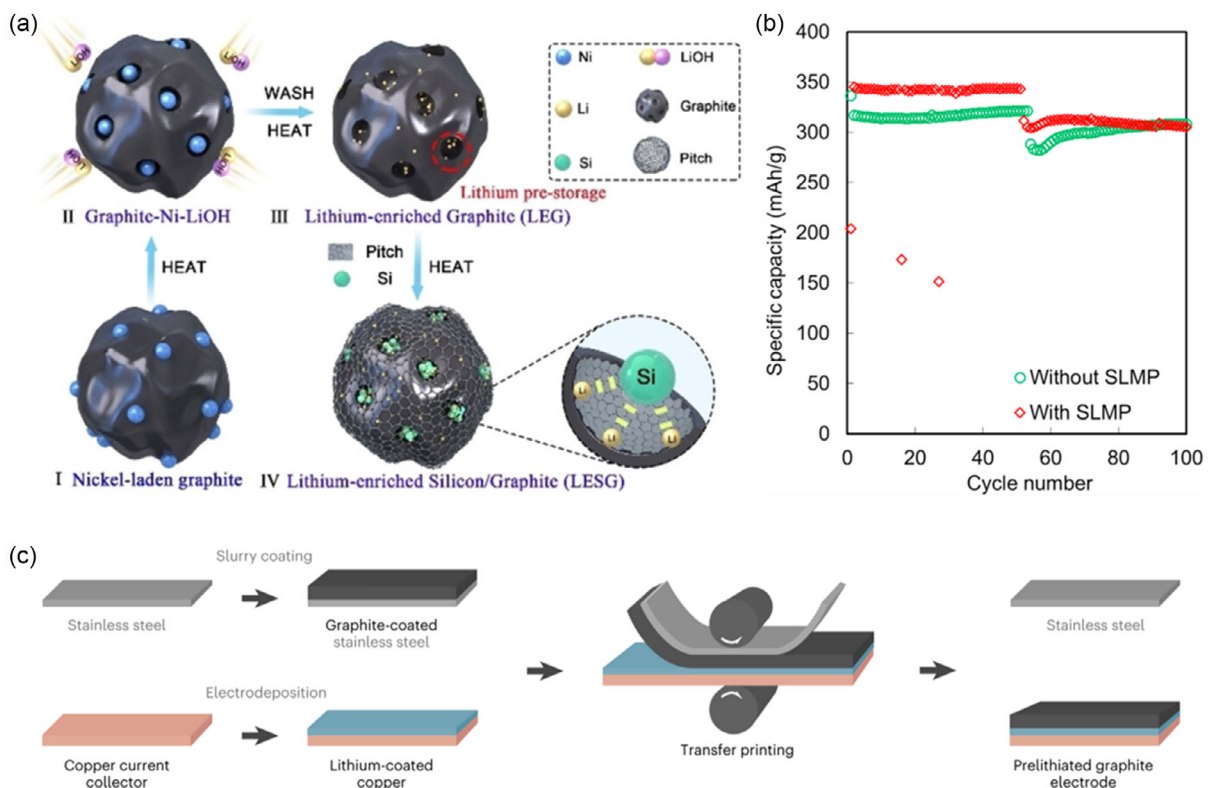


Figure 3. a) Schematic illustration for the fabrication of LESG. Reproduced with permission.^[91] Copyright 2024, John Wiley and Sons. B) Cycle performance for the graphite half-cell with SLMP and without SLMP at different rates: C/10 for the first 50 cycles and C/3 for 51 to 100 cycles. Reproduced with permission.^[92] Copyright 2014, Elsevier. c) Schematic illustration for the fabrication of preGr electrode. Reprinted under the terms of the CC-BY license.^[93] Copyright 2023, Springer Nature.

30% of the graphite capacity, exhibited superior electrochemical performance, demonstrating the potential of roll-to-roll pre-lithiation as an industrially viable strategy.

These studies collectively highlight the diverse approaches to anode pre-lithiation, each with its own advantages. Chemical pre-lithiation through LESG synthesis ensures a homogenous Li distribution and long-term cycling stability, whereas SLMP-based pre-lithiation provides a simpler yet effective way to mitigate initial capacity loss. Meanwhile, the roll-to-roll method offers a scalable solution with high initial efficiency, making it a promising candidate for large-scale manufacturing. By leveraging these pre-lithiation strategies, future advancements in anode design could further enhance the performance and commercial viability of next-generation LIBs.

3.2. LM@Capacity-G

In conventional LIB research, Li plating on graphite is considered a degradation phenomenon.^[42,43,94] However, a controlled amount of Li plating could overcome the capacity limitations of graphite and enable higher EDs.^[95] Recent studies have demonstrated the reversibility of Li plating on graphite by implementing a tailored electrolyte strategy that effectively harnesses this process to provide additional capacity.^[41,44,96] Electrolytes can be categorized into liquids and other types (including gel and solid electrolytes). Because Li plating cannot be completely controlled solely by the

electrolyte, some strategies involve the design of additional materials on the electrode. Note that Li plating for additional capacity can be induced by the cutoff conditions and full-cell design. In a half cell test, the capacity cutoff condition (e.g., up to 600 mAh g⁻¹) can be used for Li plating. In a full-cell test, the N/P ratio under 1 condition (considering only the capacity of graphite as the negative electrode) was used for Li plating.

3.2.1. Electrolyte

Recent studies have extensively explored electrolyte engineering strategies to optimize Li plating behavior on graphite-based anodes. These investigations have primarily focused on modulating the electrolyte composition such as salt type, solvent system, and additives to control the Li deposition process and suppress dendrite formation.

Cai et al. compared and described two cells fabricated using a conventional concentrated electrolyte (CCE) and an LHCE.^[97] Similarly, Yue et al. observed the behavior of Li plating on a graphite anode using a regular-concentration electrolyte (RCE) and an LHCE.^[98] The CCE and RCE are Li hexafluorophosphate (LiPF₆)-based electrolytes, whereas the LHCE is a Li bis(fluorosulfonyl)imide (LiFSI)-based electrolyte. A cell with a LiPF₆-based electrolyte forms Li dendrites primarily on the upper surface, owing to the severely localized concentration of Li and uneven distribution resulting from SEI reconstruction. When such cycles are repeated, dead Li is

formed and polarization occurs (Figure 4a: upper row; Figure 4b: right column). The cell with the LiFSI-based electrolyte suppressed dendrite formation and allowed for uniform Li distribution because both the surface and cross section were homogeneous owing to the formation of a LiF-rich SEI layer. Additionally, a sufficient reaction area and ion transport activity inside the anode were guaranteed (Figure 4a: lower row; Figure 4b: left column). During Li stripping, cells using LiPF₆-based electrolytes still exhibited irreversible Li, whereas cells employing LiFSI-based electrolytes exhibited a small amount of irreversible Li. Consequently, cells using LiFSI-based electrolytes inhibited dendrite formation better than those using LiPF₆-based electrolytes and enabled uniform Li plating.

Xu et al. demonstrated a Li-G anode with a carbonate-based electrolyte and triglyme (G3)-LiNO₃ synthetic additive (GLN).^[99] An electrolyte containing GLN forms a Li₃N-rich and elastic SEI,

thus achieving reversible Li plating. LiNO₃ acts as a precursor for the formation of Li₃N, which exhibits high thermodynamic stability and excellent Li-ion conductivity and serves as a crucial component in the SEI of a high-performance LM anode. Figure 4c shows the results of the investigation of the Li distribution in the graphite anode through time-of-flight secondary ion mass spectrometry (TOF-SIMS). After Li plating, the electrode with GLN exhibited uniform Li distribution, whereas the electrode without GLN exhibited a large concentration of Li in a localized region. The cells with GLN as an additive showed improved capacity at high rates and induced uniform Li deposition.

Expanding on the role of solvent composition, Liang et al. compared ethylene carbonate (EC)-based and EC-free electrolytes.^[100] EC is considered to be a Li dendrite inducer as it enables the formation of reducing products such as Li ethylene decarbonate

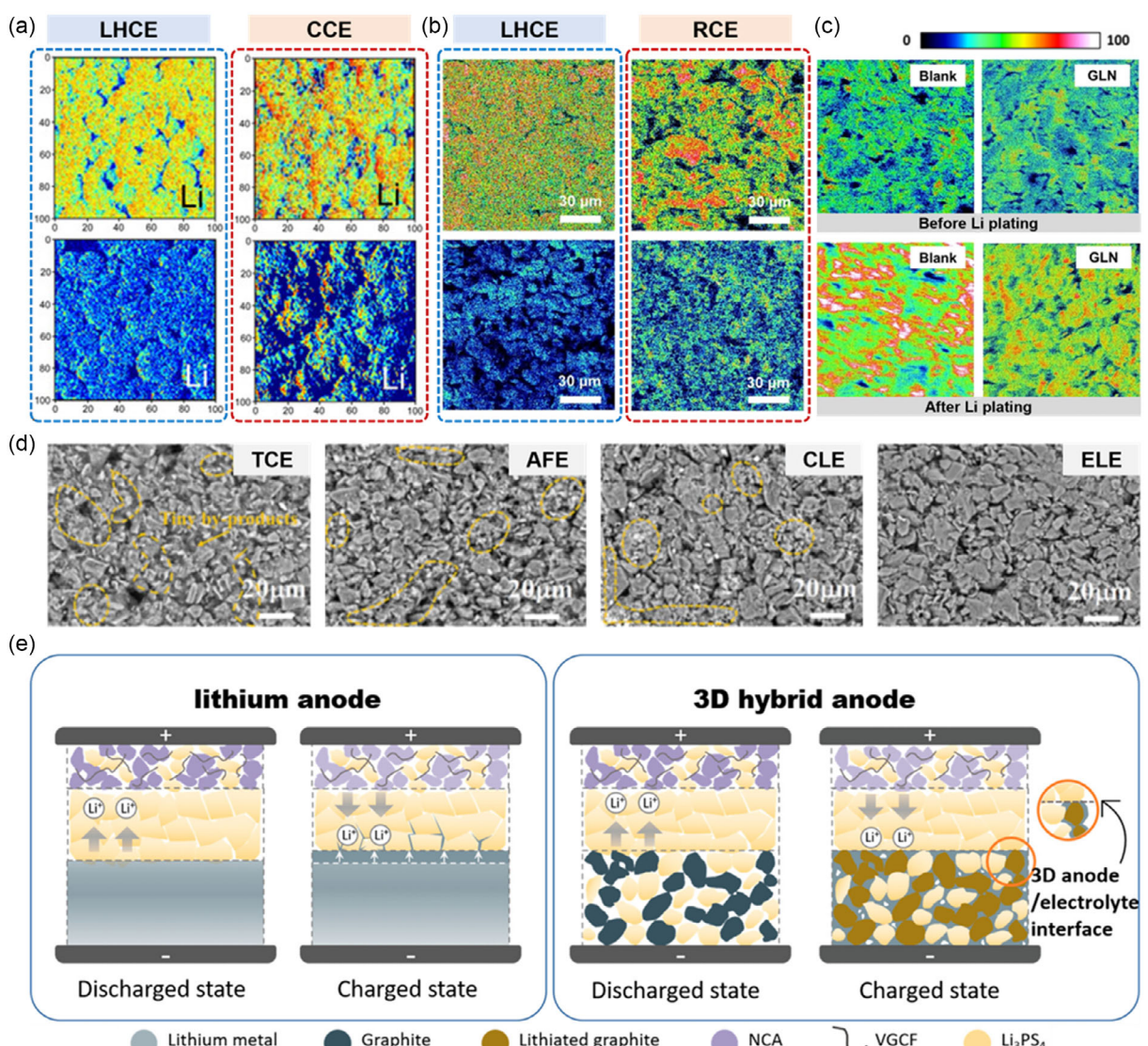


Figure 4. TOF-SIMS mapping of graphite (G) electrode a) with LHCE (left column) and CCE (right column) after plating/stripping. Reproduced with permission.^[97] Copyright 2021, John Wiley and Sons. b) With LHCE (left column) and RCE (right column) after plating/de-intercalating. Reproduced with permission.^[98] Copyright 2023, John Wiley and Sons. c) Without GLN (left column) and with GLN (right column) before/after plating (upper/lower row). Reproduced with permission.^[99] Copyright 2023, John Wiley and Sons. d) SEM image of graphite electrode with TCE, AFE, CLE, and ELE electrolytes. Reproduced with permission.^[100] Copyright 2023, Elsevier. e) Schematic illustration of an all-solid-state battery with Li metal anode (left) and 3D hybrid anode (right). The 3D hybrid anode is composed of graphite (G) and LPS. Reprinted with permission.^[102] Copyright 2021, American Chemical Society.

(Li₂EDC). Dendrites with high reaction activity and surface area undergo side reactions such as the consumption of electrolytes, leading to the generation of combustible gas. In contrast, EC-free electrolytes such as all-fluorinated electrolytes (AFEs), HCEs, and LHCEs exhibit highly reversible insertion, smooth LM deposition, and oxidation stability at high voltages. Traditional carbonated electrolytes (TCEs), AFE, carbonate-based LHCE (CLE), and ether-based LHCE (ELE) are composed of 1 M LiPF₆ in EC/dimethyl carbonate (DMC)/ethyl methyl carbonate (EMC) (1:1:1 by weight ratio) with 1% vinylene carbonate (VC), 1 M LiPF₆ in 3,3,3-fluoroethylmethyl carbonate/fluoroethylene carbonate (FEC)/(2,2,2-trifluoroethoxy)-1,1,2,2-tetrafluoroethane (HFE) (6:2:2 by weight ratio) with 0.02 M Li difluoro(oxalate)borate (LiDFOB), 1.4 M LiFSI in DMC/FEC/1,1,2,2-tetrafluoroethyl-2,2,3,3-tetrafluoropropylethane (TTE) (2:0:2:3 by mol), and 1.5 M LiFSI in DME/HFE (1:2 by volume ratio), respectively. When examining the surface with 10% Li plating using TCE, AFE, CLE, and ELE through scanning electron microscopy (SEM) images, TCE showed a significant presence of parasitic substances attached to the surface, whereas AFE, CLE, and ELE produced smaller amounts of byproducts (Figure 4d). Parasitic substances deplete the electrolyte and active Li, leading to increased resistance and negatively impacting the cycling performance. However, the use of EC-free electrolytes leads to uniform Li plating/stripping, thereby reducing the amount of residual Li. In addition, when ELE was used in a graphite anode with 20% Li plating, the initial specific capacity was 405.6 mAh g⁻¹, and the capacity retention after 200 cycles was 94.7%. However, when the TCE was used, the capacity retention was 78.9%. The use of EC-free electrolytes, such as fluorinated solvent-based systems (AFE, HCE, and LHCE), significantly reduced parasitic reactions and improved long-term cycling stability.

Konz et al. presented an equation for calculating the onset of plating based on a curve illustrating the extent of irreversible Li plating relative to the rate, temperature, and loading.^[101] The results showed the effects of different amounts of FEC on irreversible plating. Increasing the FEC content in the electrolyte delayed the onset of plating. Dead Li was suppressed as the amount of irreversible Li was reduced. When the calculated reversibility of Li plating was illustrated for various ratios of FEC in the electrolytes, the FEC-free electrolyte was expected to exhibit the lowest Li reversibility. Additionally, the reversibility of all the electrolytes was expected to decrease as the plating amount and C-rate increased. FEC was expected to delay the initiation of Li plating and prevent the formation of dead Li particles. This study provides a theoretical framework for understanding the electrolyte-plating relationship, complementing the experimental results from the aforementioned works. Their findings suggest that optimizing electrolyte additives rather than solely focusing on salt or solvent composition can be a key strategy in extending battery lifespan.

Martin et al. observed the behavior of hybrid cells in a liquid electrolyte by controlling its components: salt, solvent, and additive.^[45] A hybrid cell refers to a cell that achieves a part of its capacity through Li plating. LDBF (1 M LiDFOB + 0.4 M LiBF₄ in FEC:diethyl carbonate [DEC] [v/v = 1:2]) is an electrolyte that uses a solvent of FEC:DEC (1:2 volume ratio) in a salt mixture of 1 M LiDFOB and 0.4 M Li tetrafluoroborate (LiBF₄). And, 2F1L and

2VC are electrolytes prepared by adding 2 wt% VC and 2 wt% FEC + 1 wt% Li difluorophosphate to 1.5 M LiPF₆ in EC/EMC/DMC (25:5:70), respectively. A cell utilizing 1.5 M LiPF₆ as the salt exhibited a capacity retention decay to less than 80% before 15 cycles, and a cell employing LDBF experienced a capacity retention decrease to less than 80% after 160 cycles. The enhanced capacity retention observed in the cell fabricated with the LDBF confirmed its suitability as an electrolyte in the hybrid structure. Their research bridges the gap between traditional liquid electrolytes and hybrid architectures, providing insight into how electrolyte design can be tailored for high-performance applications.

Heterogeneous Li deposition promotes Li dendrite growth, increases the internal resistance owing to dendrite formation, and leads to the accumulation of dead Li during repeated cycles of plating and stripping, significantly degrading the battery performance. By optimizing the composition of the liquid electrolyte in terms of salt, additives, and solvent, the indiscriminate consumption of finite Li ions can be mitigated, leading to a reduction in the interfacial polarization and minimization of the formation of Li dendrites and dead Li.

Previous studies have demonstrated that optimizing liquid electrolytes through careful selection of salts, solvents, and additives can effectively regulate Li plating behavior and suppress dendrite growth. However, in addition to electrolyte engineering, another promising approach involves modifying the electrode structure itself to achieve more uniform Li deposition. Xing et al. fabricated a 3D anode by mixing Li thiophosphate (LPS), which is a solid electrolyte, with graphite.^[102] Figure 4e shows an all-solid-state battery with LM as the anode on the left side. Li deposition was initiated at the interface between the anode and the solid-state electrolyte (SSE) layer. This evolves into a structure that intercalates between the SSE layers to form dendrites. If this reaction continues, the dendrites may extend to the cathode, resulting in a short circuit, which is a critical issue for battery operation. The right side schematic in Figure 4e shows a battery constructed using a 3D anode. Owing to the presence of empty spaces between the graphite and LPS, Li deposition can occur at a location farther away from the anode and SSE layer interface, which alleviates dendrite formation. In the half cell test with a plating capacity of 0.25 mAh cm⁻², the 3D anode half cell (Li-3D cell) can undergo up to 60 cycles without a short circuit, whereas the Li-Cu cell experiences a short circuit after only 22 cycles. Additionally, at plating capacities of 0.5 and 0.75 mAh cm⁻², the Li-3D cell cycled for more than 40 cycles without shorting, whereas the Li-Cu cell experienced hard shorts at 16 and 8 cycles, respectively. Therefore, 3D anodes include space for Li deposition to address problems such as Li dendrite formation, volume changes, and short circuits, ultimately mitigating the reduction in battery life. These findings highlight that both electrolyte engineering and electrode architecture modification offer complementary strategies for achieving stable Li plating.

3.2.2. Active Material Modification

In recent years, various strategies have been explored to improve the Li plating behavior on graphite-based anodes, addressing

issues such as dendrite formation, dead Li accumulation, and cycling stability. One approach involves modifying the surface chemistry of graphite to regulate Li-ion flux and enhance uniform Li deposition.

Song et al. proposed a strategy for coating an ethylene-vinyl alcohol copolymer film on a graphite surface as an anode material (G-OH) using the spray-drying method (Figure 5a).^[103] The OH group of EVOH is lithiophilic, which controls Li⁺ flux distribution and induces uniform Li deposition. The electrolyte used was 1 M LiPF₆ in EC/DEC (1:1 weight ratio) with 5 wt% FEC. The discharge capacity of the anode in the half cell was 600 mAh g⁻¹ (3 mAh cm⁻²). As shown in the SEM image after 50 cycles, the graphite had a lot of dead Li and formed a thick dead Li layer (30 µm), whereas G-OH showed few dead Li. In G-OH, Li was fully accommodated within the porous structure of the G-OH host, which can be attributed to the passivation effect of the EVOH layer. Additionally, the lithiophilic OH group of the EVOH layer effectively regulated the flux of Li ions, resulting in a more uniform Li behavior. The cycling stability of symmetric cells with bare G or G-OH anodes was evaluated under 1 and 0.5 mAh cm⁻² conditions, with both anodes pre-deposited with a fixed Li capacity of 600 mAh g⁻¹. The G-OH symmetric cell exhibited stable cycling with a flat voltage plateau for over 500 h. In contrast, the symmetric cell with bare G showed noticeable polarization within 100 h and ultimately failed after ≈290 h, highlighting its comparatively shorter lifespan. Consequently, the challenges associated with dendrite control and dead Li accumulation were effectively mitigated.

Beyond surface modifications, structural engineering of the anode has also been investigated as an effective means to achieve

uniform Li plating. Son et al. conducted an electrochemical experiment to achieve uniform plating on Si-coated graphite using a gel electrolyte.^[34] A porous anode was designed by applying a lithiophilic layer on pristine graphite and using an organogel electrolyte, called a Si/G@gel electrode. An electrode fabricated using pristine graphite with a liquid electrolyte was called a G@liquid electrode. The liquid electrolyte consisted of 1.3 M LiPF₆ in EC:EMC:DEC (3:5:2) with 0.2 wt% LiBF₄, 10 wt% FEC, and 0.5 wt% VC additives. The organogel electrolyte was formulated by combining a liquid electrolyte with a 2 wt% cyanoethyl polyvinyl alcohol polymer. The gel electrolyte was used to assemble the cells. Following assembly, the cells underwent electrochemical testing after being conditioned for 12 h at 60 °C. Figure 5b shows the schematic and SEM images of the G@liquid and Si/G@gel electrodes before and after cycling. After 20 cycles, 30 µm of dead Li and SEI were formed in the G@liquid electrode. In contrast, after 50 cycles, the Si/G@gel electrode did not exhibit dead Li or the SEI. The Li plating on the Si/G@gel and G@liquid electrodes was denoted as Li/Si/G@gel and Li/G@liquid electrodes, respectively. The first reversible capacity and ICE of the Li/Si/G@gel and Li/G@liquid electrodes were 551.0 mAh g⁻¹ and 97.84% and 520.9 mAh g⁻¹ and 86.82%, respectively. Moreover, cycling tests with 600 mAh g⁻¹ at 0.5C further demonstrated the stability of the Li/Si/G@gel electrode. While the Li/G@liquid electrode failed within the first 20 cycles, the Li/Si/G@gel electrode exhibited exceptional capacity retention over 200 cycles, maintaining 100% of its capacity with a CE exceeding 99%. When a porous anode of Si-coated graphite with a gel electrolyte was used, the behavior of the Li plating was reversed. This demonstrates that Si alloys, graphite intercalation, and Li plating can be utilized to effectively store energy.

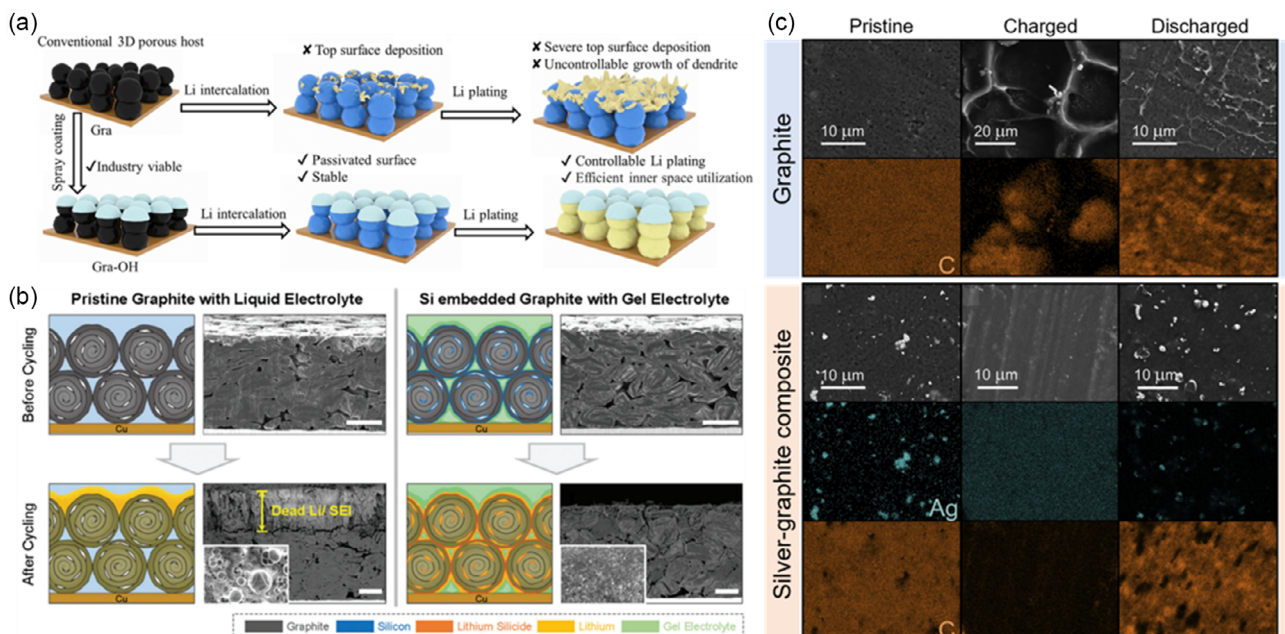


Figure 5. a) Schematic illustration of the Li plating on conventional 3D porous host and Gra-OH. Reproduced with permission.^[103] Copyright 2024, Elsevier. b) Schematic and cross-sectional SEM images of pristine G with liquid electrolyte and Si-embedded G with gel electrolyte. G electrode before cycling (upper row) and Si/G electrode after 20 cycling and 50 cycling (lower row). Reprinted under the terms of the CC-BY license.^[34] Copyright 2020, Royal Society of Chemistry. c) SEM and energy dispersive X-ray spectroscopy (EDX) mapping of G and Ag-G surface. Reprinted under the terms of the CC-BY license.^[104] Copyright 2023, Elsevier.

In addition to chemical and structural modifications, incorporating conductive interlayers has been explored to further optimize Li plating and stripping behavior. Spencer-Jolly et al. discussed the phases formed during charging and discharging in an Ag-graphite composite using a solid electrolyte and observed the changes to its surface.^[104] The anode consisted of a Li₆PS₅Cl solid electrolyte and a Ag-graphite interlayer. After charging up to a capacity of 2 mAh cm⁻² with a current density of 0.1 mA cm⁻², the composite layer in contact with the current collector was analyzed using SEM and energy dispersive X-ray spectroscopy after removing the current collector (Figure 5c). When the graphite was charged, LM was deposited in a honeycomb form and remained even after discharge. After full charging, the Ag-graphite composite was composed of Li₁₀Ag₃ and Li. After discharging, most of the Li₁₀Ag₃ returned to graphite. This indicates that the presence of Ag nanoparticles (Ag NPs) allowed the LM and Li₁₀Ag₃ alloy layers to manifest uniformly on the graphite layer and return during discharge.

These studies collectively highlight the diverse approaches to enhancing Li plating behavior on graphite-based anodes. Surface modifications, structural engineering, and conductive interlayers each contribute to mitigating issues such as dendrite growth, dead Li accumulation, and cycling instability. By integrating these strategies, future research can further refine anode design to achieve high capacity and long-cycle-life LIBs.

3.3. G@Matrix-LM

The G@Matrix-LM stores energy in the form of LM, with graphite primarily serving as a protective layer that facilitates stable Li plating/stripping reactions.^[105,106] The graphite layer enhances the stability and cycling performance by suppressing the formation of unstable SEI and Li dendrites. The Li ions stored in graphite contribute only a small fraction to the total capacity of the Li-ion cells. This section introduces studies that emphasize the role of graphite as a protective layer rather than its contribution to the overall capacity.

A silver rod was used to remove the oxide layer and impurities from the LM surface, followed by the deposition of a 50 nm Ag layer via vacuum evaporation. Graphite was then applied using a pencil core, ensuring uniform coverage on the Ag-coated Li surface with light force. The graphite loading was \approx 0.21 mg cm⁻², with a micron-scale thickness (Figure 6a).^[107] SEM analysis revealed significant differences in surface stability between the pristine Li anode and the Ag-Graphite@Li anode after cycling. In the pristine Li anode, uneven Li plating and stripping after 10 cycles resulted in a loose, porous structure with fine cracks on the electrode surface. As cycling progressed to 50 cycles, large cracks formed, and a substantial amount of dead Li accumulated, further deteriorating the electrochemical performance. In contrast, the Ag-Graphite@Li anode maintained a much more stable surface. After 10 cycles, the anode surface remained smooth, with

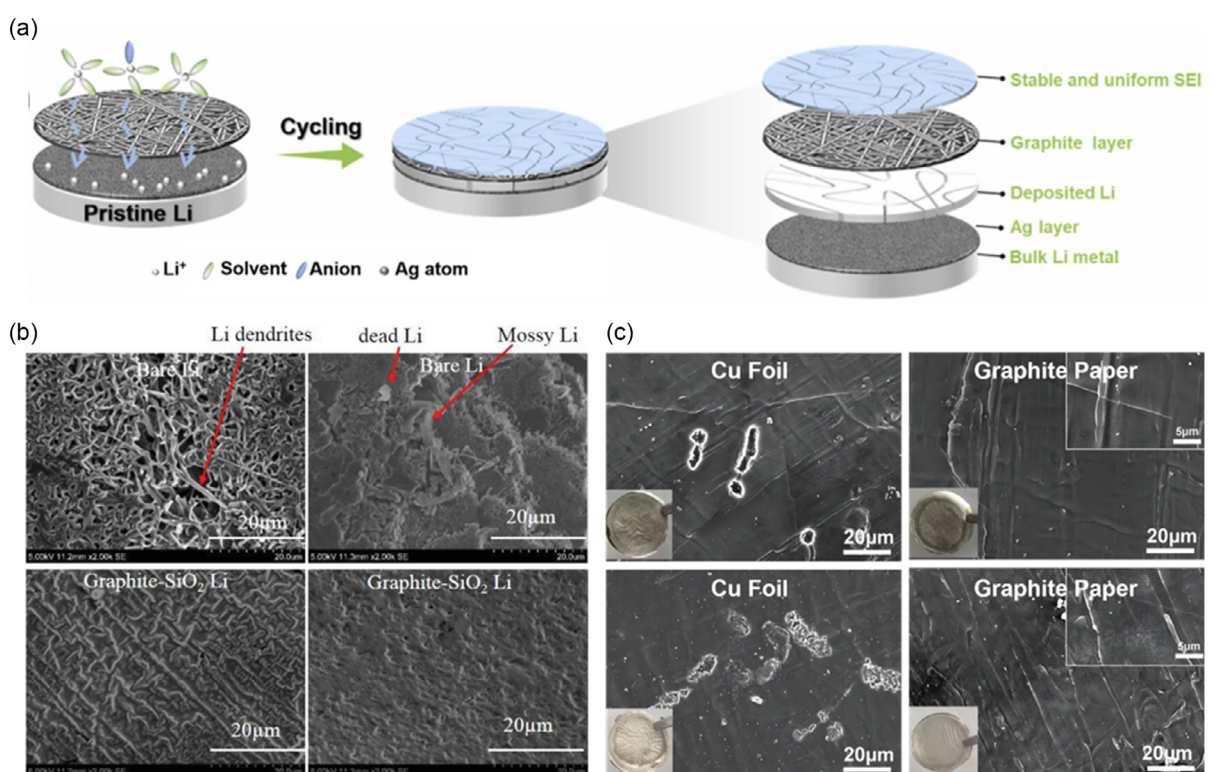


Figure 6. a) Schematic illustration of Li metal anode coated by Ag and graphite layer. Reproduced with permission.^[107] Copyright 2025, Elsevier. b) SEM images of bare Li and G-SiO₂ Li surface after 1st (left column) and 100th plating (right column). Reproduced with permission.^[108] Copyright 2019, John Wiley and Sons. c) SEM images of Li foil in the carbonate electrolyte for 7 days (upper row) and 30 days (lower row) with Cu foil and GP as the substrate. Reproduced with permission.^[109] Copyright 2023, John Wiley and Sons.

no visible Li dendrites or dead Li. Even after 50 cycles, the anode surface remained flat, with no significant dendrite growth or dead Li formation. This improved stability can be attributed to the synergistic effects of the Ag NPs and the graphite layer. The lithophilic Ag NPs promoted uniform Li deposition, preventing dendrite growth, while the graphite layer facilitated stable Li^+ transport and contributed to the formation of a robust SEI layer. Together, these factors stabilized the electrode–electrolyte interface, ensuring smooth Li plating and stripping, ultimately enhancing the cycle life of the Ag-Graphite@Li anode. Two anodes were assembled into symmetrical cells at 1 and 1 mAh cm^{-2} . The pristine Li anode showed stable cycling for 1000 h before polarization increased, while the Ag-Graphite@Li anode maintained stability or 2200 h, demonstrating a longer cycle life.

Pathak et al. investigated the impact of a graphite– SiO_2 (G– SiO_2) ultrathin bilayer on the protection of the LM surface during the charging and discharging processes.^[108] Graphite supported electron transfer between the plated Li and Li electrode, reduced impedance during Li plating/stripping, and served as a buffer for volume changes. The ultrathin SiO_2 layer promoted Li-ion diffusion and lithiation/delithiation while effectively inhibiting dendrite growth. This was achieved with high electrical conductivity, high Young's modulus, and excellent chemical stability. In Figure 6b, the SEM images of the bare Li and G– SiO_2 Li are presented after 1 cycle (left column) and 100 cycles (right column). The bare Li exhibited nonuniform deposition, a partially high electric field, and a high Li-ion flow that accelerates nucleation and growth, leading to dendrite formation and poor CE. Meanwhile, the G– SiO_2 Li exhibited a smooth surface without dendrites and featured uniform deposition, attributed to the consistent distribution of SiO_2 and gradual growth of dendrites during continuous lithiation/delithiation. As a result, the superior stability of G– SiO_2 Li was further validated in symmetric coin cells for corrosion studies. The bare Li symmetric cell exhibited a rapid overpotential increase and failed after 200 h at 1 mA cm^{-2} , whereas the G– SiO_2 Li symmetric cell maintained stable operation for over 800 h under the same conditions. Furthermore, the G– SiO_2 Li cell exhibited lower voltage hysteresis throughout cycling compared to bare Li, underscoring its enhanced electrochemical stability and extended lifespan.

Li et al. introduced and analyzed the use of graphite paper (GP) as a current collector instead of Cu foil for LM.^[109] Cu foils are widely used as current collectors in anodes. However, owing to galvanic corrosion, an undesirable phenomenon occurs between the LM and Cu foil; therefore, GP was used as the current collector. The interface between the Li foil and the GP current collector is stable and has the advantage of preventing galvanic corrosion and electrolyte decomposition problems. An ultrathin Li foil supported by GP (Li@GP) is presented, where the GP serves as the current collector for the LM. Cells with Li@GP were assembled to investigate their potential for achieving long-term stable cycling, demonstrating improved electrochemical performance. The GP and copper foil had densities of 1.8 and 7.6 g cm^{-3} , respectively. Therefore, when GPs are used as current collectors under the same conditions, a higher ED can be achieved. Additionally, the Li intercalation capacity of GP was 37 mAh g^{-1} , which is $\approx 10\%$ of that of graphite (370 mAh g^{-1}). This presents an advantage because even a small capacity from

the GP can be a valuable contribution. After immersing the Li@Cu and Li@GP electrodes in the carbonate electrolyte, we observed changes at room temperature, providing insights into the behavior of the LM on both the Cu foil and GP current collector surfaces (Figure 6c). After 7 d, holes and cavities appeared at the interface between Li and Cu, and their sizes and depths increased further after 30 d. This indicates that in LM batteries, the Cu foil undergoes galvanic corrosion when in prolonged contact with the electrolyte. However, no changes were observed in the Li@GP electrode after 7 and 30 d. Even at a high current density of 1.0 mA cm^{-2} , the Li@GP half-cell maintains stable voltage polarization for 300 h of cycling. In contrast, the Li@Cu half-cell experiences a sharp voltage rise within 220 h due to increased internal resistance, resulting from the loss of electrical contact between the Li and Cu foils. Thus, GP provides the benefits of high conductivity, excellent mechanical and chemical stability, and galvanic corrosion inhibition. The experimental results demonstrated the advantages of using GP rather than Cu foil as a current collector for LM anodes, particularly in terms of enhancing the cycle stability and ED.

Collectively, these studies highlight the versatile role of graphite in stabilizing LM anodes. Whether utilized as a surface protection layer, integrated within a bilayer system, or serving as a current collector, graphite-based approaches have consistently demonstrated improvements in Li deposition uniformity, dendrite suppression, and long-term cycling stability. These findings underscore the importance of designing multifunctional electrode architectures that leverage graphite's electrical conductivity, mechanical robustness, and chemical stability to enhance the performance of LM batteries.

4. Full-Cell Performance of Hybrid Li-G Systems

Table 1 shows the recent progress in the full-cell performance of hybrid Li-G systems. The performance results are divided based on the three categories. Pre-lithiated cells typically show a high ICE in full-cells. For instance, Yang et al. demonstrated that a full-cell pre-lithiated anode has a higher ICE than a bare anode.^[94] LiFePO₄ (LFP) and NCM111 (NCM) paired with a graphite anode (G/LFP and G/NCM, respectively) exhibited ICEs of 79.91% and 93.10%, respectively, and GED of 264.7 and 363.8 Wh kg^{-1} , respectively. The LFP and NCM full-cells paired with a 30preG anode (30preG/LFP and 30preG/NCM) exhibited ICEs of 95.88% and 89.39%, respectively, with GED of 30preG/LFP, and 30preG/NCM is 329.6 and 380.2 Wh kg^{-1} . Pre-lithiated anodes paired with various cathodes (LFP and NCM) exhibited a high ICE.

In the case of LM@Capacity-G, various approaches have been explored, including 1) full-cell with N/P ratio (based on only the capacity of graphite, excluding the capacity of Li plating) ≤ 1 induced Li plating and 2) designing full-cells based on the results from inducing Li plating in half cells (considering both the capacities of the graphite and Li plating). These different designs and electrode strategies can yield diverse effects on the cell performance. For instance, Dahn et al. achieved an ED of

Table 1. Full-cell parameters.

	Anode material	Cathode material	ICE [%]	N/P	Areal capacity [mAh cm ⁻²]	Loading level [mg cm ⁻²]	Energy density [Wh kg ⁻¹ , Wh L ⁻¹]	Retention [%]	Ref.
LM@ Prelihi-G	Graphite with SLMP	NCM111	–	–	–	6 (a) ^{a)}	–	93.2	[92]
	30preG	NCM111	89.39	1.1	–	10 (c)	–	(195th)	
		LFP	95.88	1.1	–	3 (a)	380.2	79.6	[93]
LM@ Capacity-G	Graphite	NCM523	94.5	0.82	1.85	–	–	80.2	[97]
	Graphite	LFP	–	0.8	–	–	–	80	[98]
	Graphite	LiFePO ₄	–	0.8	2.1	9.4 (a)	–	82	[99]
	Graphite	NCM622	–	0.92	–	13.8 (c)	–	(500th)	
	Graphite	NCM523	–	0.83	3.35 (a)	8 (a)	300.5	93.2	[100]
					2.80 (c)	15 (a)	779.3	(200th)	
G@Matrix-LM	Graphite	NCM523	–	0.6	–	5.07 (a)	363.17, 890	–	[101]
	Graphite/LPS	LiNb ₃ O coated NCA	–	–	–	–	141.4	70	[45]
	Li/Si/G@gel	LCO	87.8	1.05	3.3 (a)	23 (c)	474.0, 912	38.5	[102]
	Gra-OH/Li	LFP	–	1.19	–	10.5 (c)	–	74	[34]
	Graphite-SiO ₂ Li metal (bilayer)	LTO	–	–	–	2 (c)	–	(80th)	
		NCM111	84.34	–	–	9.98 (c)	–	87.6	[108]
Li@GP	Li@GP	NCM811	–	2	4.00 (c)	–	–	74.21	(400th)
						–	–	(150th)	
						–	–	80	[109]
^{a)} (a) = anode; (c) = cathode.									

363.17 Wh kg⁻¹ and 890 Wh L⁻¹ by employing a strategy that induced Li plating through setting N/P ratio to 0.6.^[45] Son et al. designed a full-cell with electrodes that induced Li plating in a half cell. The LiCoO₂ (LCO) paired with the prepared anode had an N/P ratio of 1.05.^[34] The capacities of the Li/G@liquid and Li/Si/G@gel electrodes were 118.8 and 126.5 mAh g⁻¹, respectively, and reported ICEs of 85.9% and 87.8%, respectively. The Si/G@gel electrode with Li plating showed better capacity and ICE. The Li/Si/G@gel electrode achieved a high ED of 747.0 Wh kg⁻¹ and 912.0 Wh L⁻¹.

When employing the G@Matrix-LM strategy, the N/P ratio tends to be relatively high compared with that in other systems owing to the utilization of excessive amounts of LM. Li et al. adopted a full-cell design with an N/P ratio of 2;^[109] the cathode used NCM811 with 4 mAh cm⁻². The Li@GP electrode showed a high initial discharge capacity of 193.5 mAh g⁻¹, the capacity decreased to 154.5 mAh g⁻¹ with a retention of 80% after 160

cycles. In contrast, the capacity retentions of the bare Li and Li@Cu electrodes were 80% (after 81 cycles) and 80% (after 94 cycles), respectively. The compatibility of the LM and GP works well even in full-cells, providing stable long-term cycling performance. Although various hybrid Li-G systems have been explored, most studies have not comprehensively addressed all the factors presented in Table 1. By delineating all the aforementioned factors, not only will more precise comparisons between papers become feasible, but this will also facilitate advancements in the field of LIBs.

5. Summary and Outlook

In this review, we classify electrodes that incorporate both Li and graphite into three categories based on the predominant Li storage mechanism during cycling and discuss the strategies for

each. 1) LM@Prelithi-G: a system that improves the ICE through pre-lithiation and utilizes capacity through the intercalation/deintercalation of graphite. 2) LM@Capacity-G: a system that utilizes the capacity of both graphite and Li by enabling the intercalation/deintercalation of graphite and plating/stripping of LM. It is categorized according to the type of electrolyte used. Because the degradation mechanisms of the Li plating/stripping reaction cannot be entirely prevented with the electrolyte alone, additional strategies have been used, such as the use of a lithophilic layer. 3) G@Matrix-LM: a system that employs a small quantity of graphite as a protective layer to mitigate the irreversible behavior of the LM. Various techniques, such as layer coating and current collectors, have been proposed to address the limitations associated with LM.

Each system exhibits varying performance changes, and given the diverse strategies needed for improvement, achieving enhanced performance requires appropriate strategies tailored to each system.

We presented a hybrid Li-G system for batteries with a high ED. In the hybrid Li-G system, pre-lithiated graphite was applied to the current commercial LIB system and has the advantage of increasing the ICE. The hybrid Li-G system allows for higher EDs than the current graphite-only anodes used in LIBs. The maximum anode capacity in LIBs can be achieved by incorporating LM. However, to ensure stability in electrochemical reactions, graphite, which has a well-established track record for stability in LIBs, can be utilized as a protective layer.

Despite the promising prospects of hybrid Li-G systems, several challenges must be addressed to ensure their practical implementation in industrial applications. The scalability of pre-lithiation processes remains a significant obstacle due to its complexity, costs, and potential safety concerns. Moreover, the strategy of using high-cost electrolytes contrasts with the demand for lower battery costs, while the mechanical stability of composite electrodes has yet to be validated under practical cell configurations and operating conditions over long-term cycling. However, these hurdles are not limited to Li-G systems alone but represent common challenges shared across various next-generation anodes (e.g., LM and Si-based anodes), suggesting considerable room for improvement in the future. For example, advanced technologies for next-generation anodes, including low cost, advanced electrolytes, mechanically robust binders, and advanced electrode and cell designs, can be applied to Li-G systems to enhance their feasibility.

Thus, future research on hybrid Li-G systems focuses not merely on applying technologies developed for other next-generation anodes but rather on developing solutions specifically tailored for the commercialization of hybrid Li-G systems. For instance, it is essential to develop functional surfaces that enable more reversible Li plating, as well as promote dense Li plating to maximize Li capacity while minimizing electrode expansion during plating. Moreover, since hybrid Li-G systems utilize both intercalation and Li plating mechanisms, optimized charging protocols must be account for these dual Li reaction mechanisms.^[110] Additionally, the various Li-G hybrid concepts discussed in this work allow for customized cell designs beyond conventional full-cell design. Rather than simply targeting an N/P ratio of 1, designs

can be made where the ratio is inverted or significantly increased, enabling more anode-tailored full-cell configurations.^[111] Such focused research on Li-G systems will advance their development and potential for practical implementation.

Acknowledgements

This work was supported by the National Research Foundation of Korea (NRF) grant funded by the Korea government (MSIT) (grant no. 2022R1C1C1010303). This research received funding from the "Junior Faculty Research Support Grant" at Changwon National University in 2024.

Conflict of Interest

The authors declare no conflict of interest.

Keywords: energy densities · graphites · hybrid anodes · lithiums

- [1] M. Li, J. Lu, Z. Chen, K. Amine, *Adv. Mater.* **2018**, *30*, 1800561.
- [2] M. M. Thackeray, C. Wolverton, E. D. Isaacs, *Energy Environ. Sci.* **2012**, *5*, 7854.
- [3] B. Dunn, H. Kamath, J. Tarascon, *Science* **2011**, *334*, 928.
- [4] V. Etacheri, R. Marom, R. Elazari, G. Salitra, D. Aurbach, *Energy Environ. Sci.* **2011**, *4*, 3243.
- [5] J. B. Goodenough, *Acc. Chem. Res.* **2013**, *46*, 1053.
- [6] R. Schmuck, R. Wagner, G. Höpfl, T. Placke, M. Winter, *Nat. Energy* **2018**, *3*, 267.
- [7] Y. Zou, Z. Cao, J. Zhang, W. Wahyudi, Y. Wu, G. Liu, Q. Li, H. Cheng, D. Zhang, G. Park, L. Cavallo, T. D. Anthopoulos, L. Wang, Y. Sun, J. Ming, *Adv. Mater.* **2021**, *33*, 2102964.
- [8] J. W. Choi, D. Aurbach, *Nat. Rev. Mater.* **2016**, *1*, 16013.
- [9] Y. Cao, M. Li, J. Lu, J. Liu, K. Amine, *Nat. Nanotechnol.* **2019**, *14*, 200.
- [10] M. R. Showalter, J. J. Lissauer, *Science* **2006**, *311*, 977.
- [11] X. Gao, H. Yang, *Energy Environ. Sci.* **2010**, *3*, 174.
- [12] J. Li, Z. Du, R. E. Ruther, S. J. An, L. A. David, K. Hays, M. Wood, N. D. Phillip, Y. Sheng, C. Mao, S. Kalnaus, C. Daniel, D. L. Wood, *JOM* **2017**, *69*, 1484.
- [13] X. Shen, H. Liu, X. Cheng, C. Yan, J. Huang, *Energy Storage Mater.* **2018**, *12*, 161.
- [14] F. Wu, J. Maier, Y. Yu, *Chem. Soc. Rev.* **2020**, *49*, 1569.
- [15] B. Esser, F. Dolhem, M. Becuwe, P. Poizot, A. Vlad, D. Brandell, *J. Power Sources* **2021**, *482*, 228814.
- [16] X. Zhang, C. Zhao, J. Huang, Q. Zhang, *Engineering* **2018**, *4*, 831.
- [17] J. R. Croy, A. Abouimrane, Z. Zhang, *MRS Bull.* **2014**, *39*, 407.
- [18] X. Su, Q. Wu, J. Li, X. Xiao, A. J. Lott, W. Lu, B. W. Sheldon, J. Wu, *Adv. Energy Mater.* **2014**, *4*, 1300882.
- [19] L. Sun, Y. Liu, R. Shao, J. Wu, R. Jiang, Z. Jin, *Energy Storage Mater.* **2022**, *46*, 482.
- [20] K. Feng, M. Li, W. Liu, A. G. Kashkooli, X. Xiao, M. Cai, Z. Chen, *Small* **2018**, *14*, 1702737.
- [21] P. Li, G. Zhao, X. Zheng, X. Xu, C. Yao, W. Sun, S. X. Dou, *Energy Storage Mater.* **2018**, *15*, 422.
- [22] B. Liang, Y. Liu, Y. Xu, *J. Power Sources* **2014**, *267*, 469.
- [23] J. K. Lee, C. Oh, N. Kim, J. Hwang, Y. Sun, J. Mater. Chem. A. **2016**, *4*, 5366.
- [24] J. R. Szczech, S. Jin, *Energy Environ. Sci.* **2011**, *4*, 56.
- [25] Y. Son, J. Ma, N. Kim, T. Lee, Y. Lee, J. Sung, S. Choi, G. Nam, H. Cho, Y. J. Yoo, J. Cho, *Adv. Energy Mater.* **2019**, *9*, 1803480.
- [26] S. Cui, J. Zhang, S. Fan, X. Xing, L. Deng, Y. Gong, *Nano Lett.* **2022**, *22*, 9559.
- [27] H. Lee, J. Moon, Y. Byeon, W. Y. Yoon, H. Kim, J. Ahn, *ACS Energy Lett.* **2022**, *7*, 2469.
- [28] R. Yu, Y. Pan, Y. Liu, L. Zhou, D. Zhao, J. Wu, L. Mai, A. C. S. Nano. **2023**, *17*, 2568.
- [29] N. KLINGER, E. L. STRAUSS, K. L. KOMAREK, *J. Am. Ceram. Soc.* **1966**, *49*, 369.
- [30] I. Sheet, A. Kabbani, H. Holail, *Energy Procedia* **2014**, *50*, 130.
- [31] H. Wu, Y. Cui, *Nano Today* **2012**, *7*, 414.

- [32] H. Wu, G. Chan, J. W. Choi, I. Ryu, Y. Yao, M. T. McDowell, S. W. Lee, A. Jackson, Y. Yang, L. Hu, Y. Cui, *Nat. Nanotechnol.* **2012**, *7*, 310.
- [33] J. Sung, N. Kim, J. Ma, J. H. Lee, S. H. Joo, T. Lee, S. Chae, M. Yoon, Y. Lee, J. Hwang, S. K. Kwak, J. Cho, *Nat. Energy* **2021**, *6*, 1164.
- [34] Y. Son, T. Lee, B. Wen, J. Ma, C. Jo, Y. Cho, A. Boies, J. Cho, M. De Volder, *Energy Environ. Science* **2020**, *13*, 3723.
- [35] D. Lin, Y. Liu, Y. Cui, *Nat. Nanotechnol.* **2017**, *12*, 194.
- [36] Q. Wang, T. Lu, Y. Xiao, J. Wu, L. Guan, L. Hou, H. Du, H. Wei, X. Liu, C. Yang, Y. Wei, H. Zhou, Y. Yu, *Electrochem. Energy Rev.* **2023**, *6*, 22.
- [37] F. Ding, W. Xu, G. L. Graff, J. Zhang, M. L. Sushko, X. Chen, Y. Shao, M. H. Engelhard, Z. Nie, J. Xiao, X. Liu, P. V. Sushko, J. Liu, J. Zhang, *J. Am. Chem. Soc.* **2013**, *135*, 4450.
- [38] J. Wang, H. Hu, S. Duan, Q. Xiao, J. Zhang, H. Liu, Q. Kang, L. Jia, J. Yang, W. Xu, H. Fei, S. Cheng, L. Li, M. Liu, H. Lin, Y. Zhang, *Adv. Funct. Mater.* **2022**, *32*, 2110468.
- [39] Y. Ye, Y. Zhao, T. Zhao, S. Xu, Z. Xu, J. Qian, L. Wang, Y. Xing, L. Wei, Y. Li, J. Wang, L. Li, F. Wu, R. Chen, *Adv. Mater.* **2021**, *33*, 2105029.
- [40] J. Liu, Z. Bao, Y. Cui, E. J. Dufek, J. B. Goodenough, P. Khalifah, Q. Li, B. Y. Liaw, P. Liu, A. Manthiram, Y. S. Meng, V. R. Subramanian, M. F. Toney, V. V. Viswanathan, M. S. Whittingham, J. Xiao, W. Xu, J. Yang, X. Yang, J. Zhang, *Nat. Energy* **2019**, *4*, 180.
- [41] C. Uhlmann, J. Illig, M. Ender, R. Schuster, E. Ivers-Tiffée, *J. Power Sources* **2015**, *279*, 428.
- [42] L. Xu, Y. Xiao, Y. Yang, R. Xu, Y. X. Yao, X. R. Chen, Z. H. Li, C. Q. Yan, J. Huang, Huang, *Adv. Mater.* **2023**, *35*, 2301881.
- [43] A. J. Smith, Y. Fang, A. Mikheenkova, H. Ekström, P. Svens, I. Ahmed, M. J. Lacey, G. Lindbergh, I. Furó, R. W. Lindström, *J. Power Sources* **2023**, *573*, 233118.
- [44] X. Duan, B. Li, J. Li, X. Gao, L. Wang, J. Xu, *Adv. Energy Mater.* **2023**, *13*, 2203767.
- [45] C. Martin, M. Genovese, A. J. Louli, R. Weber, J. R. Dahn, *Joule* **2020**, *4*, 1296.
- [46] T. Gao, Y. Han, D. Fragedakis, S. Das, T. Zhou, C. Yeh, S. Xu, W. C. Chueh, J. Li, M. Z. Bazant, *Joule* **2021**, *5*, 393.
- [47] L. Ye, X. Li, *Nature* **2021**, *593*, 218.
- [48] L. Tan, L. Zhang, Q. Sun, M. Shen, Q. Qu, H. Zheng, *Electrochim. Acta* **2013**, *111*, 802.
- [49] S. Wang, D. Liu, X. Cai, L. Zhang, Y. Liu, X. Qin, R. Zhao, X. Zeng, C. Han, C. Zhan, F. Kang, B. Li, *Nano Energy* **2021**, *90*, 106510.
- [50] K. R. Tallman, B. Zhang, L. Wang, S. Yan, K. Thompson, X. Tong, J. Thieme, A. Kiss, A. C. Marschilok, K. J. Takeuchi, D. C. Bock, E. S. Takeuchi, *ACS Appl. Mater. Interfaces* **2019**, *11*, 46864.
- [51] S. Tan, Z. Shadike, X. Cai, R. Lin, A. Kludze, O. Borodin, B. L. Lucht, C. Wang, E. Hu, K. Xu, X. Yang, *Electrochem. Energy Rev.* **2023**, *6*, 35.
- [52] W. Xu, J. Wang, F. Ding, X. Chen, E. Nasibulin, Y. Zhang, J. Zhang, *Energy Environ. Science* **2014**, *7*, 513.
- [53] M. S. Whittingham, *Proc. IEEE* **2012**, *100*, 1518.
- [54] J. M. Tarascon, M. Armand, *Nature* **2001**, *414*, 359.
- [55] D. M. Piper, T. A. Yersak, S. Lee, *J. Electrochem. Soc.* **2012**, *160*, A77.
- [56] J. L. Goldman, B. R. Long, A. A. Gewirth, R. G. Nuzzo, *Adv. Funct. Mater.* **2011**, *21*, 2412.
- [57] J. Choi, K. Kim, J. Jeong, K. Y. Cho, M. Ryoo, Y. M. Lee, *ACS Appl. Mater. Interfaces* **2015**, *7*, 14851.
- [58] C. Yang, Y. Yin, S. Zhang, N. Li, Y. Guo, *Nat. Commun.* **2015**, *6*, 8058.
- [59] I. H. Son, J. Hwan Park, S. Kwon, S. Park, M. H. Rümmeli, A. Bachmatiuk, H. J. Song, J. Ku, J. W. Choi, J. Choi, S. Doo, H. Chang, *Nat. Commun.* **2015**, *6*, 7393.
- [60] T. Song, J. Xia, J. Lee, D. H. Lee, M. Kwon, J. Choi, J. Wu, S. K. Doo, H. Chang, W. I. Park, D. S. Zang, H. Kim, Y. Huang, K. Hwang, J. A. Rogers, U. Paik, *Nano Lett.* **2010**, *10*, 1710.
- [61] S. Lee, J. Lee, S. Chung, H. Lee, S. Lee, H. Baik, *J. Power Sources* **2001**, *97*, 191.
- [62] Q. Wang, B. Liu, Y. Shen, J. Wu, Z. C. Zhao, C. Zhong, W. Hu, *Adv. Sci.* **2021**, *8*, 2101111.
- [63] X. Shen, X. Cheng, P. Shi, J. Huang, X. Zhang, C. Yan, T. Li, Q. Zhang, *J. Energy Chem.* **2019**, *37*, 29.
- [64] M. T. McDowell, I. Ryu, S. W. Lee, C. Wang, W. D. Nix, Y. Cui, *Adv. Mater.* **2012**, *24*, 6034.
- [65] H. Kim, B. Han, J. Choo, J. Cho, *Angew. Chem. Int. Ed.* **2008**, *47*, 10151.
- [66] M. N. Obrovac, L. Christensen, *Electrochim. Solid-State Lett.* **2004**, *7*, A93.
- [67] C. Fang, J. Li, M. Zhang, Y. Zhang, F. Yang, J. Z. Lee, M. Lee, J. Alvarado, M. A. Schroeder, Y. Yang, B. Lu, N. Williams, M. Ceja, L. Yang, M. Cai, J. Gu, K. Xu, X. Wang, Y. S. Meng, *Nature* **2019**, *572*, 511.
- [68] B. Horstmann, J. Shi, R. Amine, M. Werres, X. He, H. Jia, F. Hausen, I. Cekic-Laskovic, S. Wiemers-Meyer, J. Lopez, D. Galvez-Aranda, F. Baakes, D. Bresser, C. Su, Y. Xu, W. Xu, P. Jakes, N. A. Eichel, E. Figgemeier, U. Krewer, J. M. Seminario, P. B. Balbuena, C. Wang, S. Passerini, Y. Shao-Horn, M. Winter, K. Amine, R. Kostecki, A. Latz, *Energy Environ. Sci.* **2021**, *14*, 5289.
- [69] Y. Tian, Y. An, C. Wei, H. Jiang, S. Xiong, J. Feng, Y. Qian, *Nano Energy* **2020**, *78*, 105344.
- [70] J. Qian, B. D. Adams, J. Zheng, W. Xu, W. A. Henderson, J. Wang, M. E. Bowden, S. Xu, J. Hu, J. Zhang, *Adv. Funct. Mater.* **2016**, *26*, 7094.
- [71] A. J. Louli, A. Eldesoky, R. Weber, M. Genovese, M. Coon, J. Degoooyer, Z. Deng, R. T. White, J. Lee, T. Rodgers, R. Petibon, S. Hy, S. J. H. Cheng, J. R. Dahn, *Nat. Energy* **2020**, *5*, 693.
- [72] R. Weber, M. Genovese, A. J. Louli, S. Hames, C. Martin, I. G. Hill, J. R. Dahn, *Nat. Energy* **2019**, *4*, 683.
- [73] S. W. Lee, M. T. McDowell, J. W. Choi, Y. Cui, *Nano Lett.* **2011**, *11*, 3034.
- [74] M. T. McDowell, S. Woo Lee, C. Wang, Y. Cui, *Nano Energy* **2012**, *1*, 401.
- [75] M. Ashuri, Q. He, L. L. Shaw, *Nanoscale* **2016**, *8*, 74.
- [76] M. T. McDowell, S. W. Lee, I. Ryu, H. Wu, W. D. Nix, J. W. Choi, Y. Cui, *Nano Lett.* **2011**, *11*, 4018.
- [77] S. Chae, M. Ko, K. Kim, K. Ahn, J. Cho, *Joule* **2017**, *1*, 47.
- [78] N. Liu, Z. Lu, J. Zhao, M. T. McDowell, H. Lee, W. Zhao, Y. Cui, *Nat. Nanotechnol.* **2014**, *9*, 187.
- [79] L. Y. Beaulieu, K. W. Eberman, R. L. Turner, L. J. Krause, J. R. Dahn, *Electrochim. Solid-State Lett.* **2001**, *4*, A137.
- [80] R. Wang, W. Cui, F. Chu, F. Wu, *J. Energy Chem.* **2020**, *48*, 145.
- [81] Y. Liu, D. Lin, Z. Liang, J. Zhao, K. Yan, Y. Cui, *Nat. Commun.* **2016**, *7*, 10992.
- [82] C. Lee, M. An, E. Kim, H. An, J. Park, C. Jo, Y. Son, *Korean J. Chem. Eng.* **2024**, *41*, 43.
- [83] N. Kim, Y. Kim, J. Sung, J. Cho, *Nat. Energy* **2023**, *8*, 921.
- [84] Y. Son, H. Cha, C. Jo, A. S. Groombridge, T. Lee, A. Boies, J. Cho, M. De Volder, *Mater. Today Energy* **2021**, *21*, 100838.
- [85] F. Holtstiege, P. Bärmann, R. Nölle, M. Winter, T. Placke, *Batteries* **2018**, *4*, 4.
- [86] F. Wang, B. Wang, J. Li, B. Wang, Y. Zhou, D. Wang, H. Liu, S. Dou, *ACS Nano* **2021**, *15*, 2197.
- [87] H. J. Kim, S. Choi, S. J. Lee, M. W. Seo, J. G. Lee, E. Deniz, Y. J. Lee, E. K. Kim, J. W. Choi, *Nano Lett.* **2016**, *16*, 282.
- [88] R. Zhan, X. Wang, Z. Chen, Z. W. Seh, L. Wang, Y. Sun, *Adv. Energy Mater.* **2021**, *11*, 2101565.
- [89] Y. F. Shen, X. H. Shen, M. Yang, J. F. L. Qian, Y. Cao, H. Yang, Y. Luo, X. Ai, *Adv. Funct. Mater.* **2021**, *31*, 2101181.
- [90] C. L. Berhaut, D. Z. Dominguez, D. Tomasi, C. Vincens, C. Haon, Y. Reynier, W. Porcher, N. Boudet, N. Blanc, G. A. Chahine, S. Tardif, S. Pouget, S. Lyonnard, *Energy Storage Mater.* **2020**, *29*, 190.
- [91] Y. Gao, C. Cui, Z. Huang, G. Pan, Y. Gu, Y. Yang, F. Bai, Z. Sun, T. Zhang, *Angew. Chem. Int. Ed.* **2024**, *63*, e202404637.
- [92] Z. Wang, Y. Fu, Z. Zhang, S. Yuan, K. Amine, V. Battaglia, G. Liu, *J. Power Sources* **2014**, *260*, 57.
- [93] C. Yang, H. Ma, R. Yuan, K. Wang, K. Liu, Y. Long, F. Xu, L. Li, H. Zhang, Y. Zhang, X. Li, H. Wu, *Nat. Energy* **2023**, *8*, 703.
- [94] S. Jamnuch, T. A. Pascal, *Nat. Commun.* **2023**, *14*, 2291.
- [95] G. Park, S. Kim, J. Kim, S. Bae, Y. Heo, D. Park, H. Kim, J. Shin, J. Moon, J. W. Choi, *Adv. Energy Mater.* **2024**, *14*, 2401289.
- [96] M. Petzl, M. A. Danzer, *J. Power Sources* **2014**, *254*, 80.
- [97] W. L. Cai, C. Yan, Y. Yao, L. Xu, X. Chen, J. Huang, Q. Zhang, *Angew. Chem. Int. Ed.* **2021**, *60*, 13007.
- [98] X. Yue, J. Zhang, Y. Dong, Y. Chen, Z. Shi, X. Z. Xu, X. Li, Z. Liang, *Angew. Chem. Int. Ed.* **2023**, *135*, e202302285.
- [99] X. Xu, X. Yue, Y. Chen, Z. Liang, *Angew. Chem. Int. Ed.* **2023**, *62*, e202306963.
- [100] H. Liang, L. Wang, Y. He, Y. Song, J. Gao, G. Xu, H. Xu, H. Zhang, X. He, *Chem. Eng. J.* **2023**, *454*, 140290.
- [101] Z. M. Konz, B. M. Wirtz, A. Verma, T. Huang, H. K. Bergstrom, M. J. Crafton, D. E. Brown, E. J. McShane, A. M. Colclasure, B. D. McCloskey, *Nat. Energy* **2023**, *8*, 450.
- [102] X. Xing, Y. Li, S. Wang, H. Liu, Z. Wu, S. Yu, J. Holoubek, H. Zhou, P. Liu, *ACS Energy Lett.* **2021**, *6*, 1831.
- [103] Z. Song, J. Xue, C. Wei, Q. Zhao, A. Zhou, J. Li, *Chem. Eng. J.* **2024**, *490*, 151618.
- [104] D. Spencer-Jolly, V. Agarwal, C. Doerr, B. Hu, S. Zhang, D. L. R. Melvin, H. Gao, X. Gao, P. Adamson, O. V. Magdysyuk, P. S. Grant, R. A. House, P. G. Bruce, *Joule* **2023**, *7*, 503.
- [105] G. Zheng, S. W. Lee, Z. Liang, H. Lee, K. Yan, H. Yao, H. Wang, W. Li, S. Chu, Y. Cui, *Nat. Nanotechnol.* **2014**, *9*, 618.

- [106] J. Wen, T. C. Wang, C. Wang, Y. Dai, Z. Song, X. Liu, Q. Yu, X. Zheng, J. Ma, W. Luo, Y. Huang, *Adv. Mater.* **2024**, *36*, 2307732.
- [107] N. Pei, J. Liu, Y. Zhang, X. Yang, Y. Deng, P. Zhang, J. Zhao, *Next Mater.* **2025**, *6*, 100468.
- [108] R. Pathak, K. Chen, A. Gurung, K. M. Reza, B. Bahrami, F. Wu, A. Chaudhary, N. Ghimire, B. Zhou, W. Zhang, Y. Zhou, Q. Qiao, *Adv. Energy Mater.* **2019**, *9*, 1901486.
- [109] Y. Li, Q. Guo, Y. Wu, D. Ying, Y. Yu, T. Chi, S. Xia, X. Zhou, Z. Liu, *Adv. Funct. Mater.* **2023**, *33*, 2214523.
- [110] Y. Zhang, W. Bao, E. Jeffs, B. Liu, W. Mai, X. Li, W. Li, Y. Xu, B. Bhamwala, A. Liu, L. Ah, K. Ryu, Y. S. Meng, H. Gan, *ACS Energy Lett.* **2025**, *10*, 872.
- [111] T. Lee, M. J. Seong, H. C. Ahn, M. Baek, K. Park, J. Oh, T. Choi, J. W. Choi, *Proc. Natl. Acad. Sci. U.S.A.* **2024**, *122*, e2417053121.

Manuscript received: December 30, 2024

Revised manuscript received: March 9, 2025

Version of record online: March 21, 2025
